Lamellar Orientation of Diblock Copolymer Solutions under Steady Shear Flow

Shinichi Kitade, Nobuo Ochiai, Yoshiaki Takahashi,*,† and Ichiro Noda

Department of Applied Chemistry, Graduate School of Engineering, Nagoya University, Nagoya 464-8603, Japan

Yushu Matsushita

Neutron Scattering Laboratory, The Institute of Solid State Physics, The University of Tokyo, Shirakata, Tokai, Naka, Ibaraki 319-1106, Japan

Alamgir Karim, Alan I. Nakatani, Hongdoo Kim,‡ and Charles C. Han

Polymers Division, National Institute of Standards and Technology, Gaithersburg, Maryland 20899

Received October 7, 1997; Revised Manuscript Received August 21, 1998

ABSTRACT: The steady shear rate dependence of the structure of two poly(styrene-d_8-*b*-2-vinylpyridine)s in α-chloronaphthalene, a common good solvent, was measured by small-angle neutron scattering (SANS) in a couette flow cell geometry in the ordered state, in which the solutions assume a lamellar structure (randomly oriented grains). SANS measurements revealed that steady shear flow induces macroscopic lamellar orientation at certain characteristic shear rates for the higher molecular weight sample (M_w = 3.6×10^5). Lamellar normals are preferentially oriented along the vorticity direction at high shear rates. However, no shear effect was observed for the low molecular weight sample ($M_w = 2.0 \times 10^5$).

Introduction

Block copolymers, which consist of mutually incompatible block components, generally exhibit a phase transition called the "order−disorder transition" (ODT) at certain temperatures. In the ordered state, diblock copolymers assume various periodic morphologies such as lamellar, bicontinuous, cylindrical, or spherical structures, depending on composition.

Recently, the effects of shear flow on the morphologies of block copolymer melts or solutions have extensively been studied.[1−19] Most of these studies have been conducted on samples exhibiting lamellar or cylindrical morphology in the quiescent state. In general, microdomain structures are assemblies of randomly oriented microdomains that are hundreds of nanometers in size, so that the scattering patterns from the microdomains are isotropic. If the microdomains (for example, lamellar domains) are oriented along a particular direction under shear flow, the oriented lamellar domains give anisotropic scattering patterns. Hereafter, as illustrated in Figure 1, we call lamellar orientations "transverse", "parallel", and "perpendicular" where the normals are oriented along the shear flow (1), shear gradient (2), and vorticity (3) directions, respectively. The experimental conditions under which the orientation occurs are determined by various factors such as temperature (T), type of flow, shear rate ($\dot{\gamma}$), frequency of oscillatory shear (ω), and strain amplitude. Besides these factors, the difference in the rheological properties of the block components may affect the lamellar orientation.

Most of these studies have been conducted under oscillatory shear flow. For lamellar structures of poly(ethylenepropylene)−poly(ethylethylene) (PEP−PEE) diblock copolymers, the "parallel" orientation was observed at low frequency, while the "perpendicular" orientation was observed at high frequency near the ODT temperature, T_{ODT}, when the strain amplitude was large (about 100%).[3] For lamellar structures of polystyrene−polyisoprene (PS−PI) diblock copolymers, on the other hand, the "parallel" orientation was observed even at small strain amplitudes (5%).[5] Moreover,

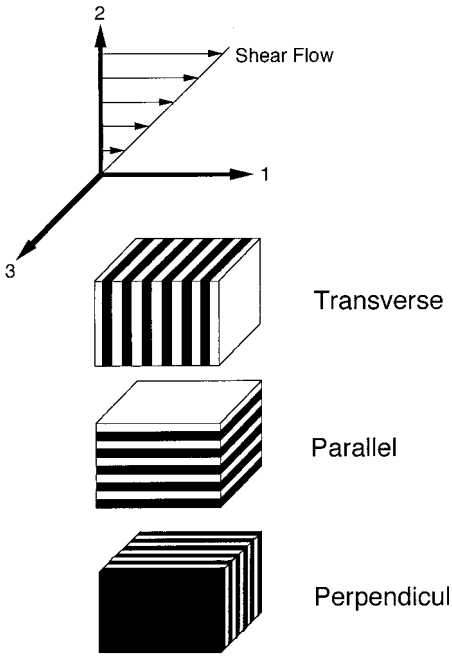

Figure 1. Schematic diagrams of the "transverse", "parallel", and "perpendicular" orientations of lamellae under shear flow. The normals of the lamellae are parallel to the shear flow, shear gradient, and vorticity direction in the "transverse", "parallel", and "perpendicular" orientations, respectively.

† Present address: Center for Integrated Research in Science and Engineering, Nagoya University, Nagoya 464-8603, Japan.
‡ Present address: Department of Chemistry, Kyunghee University, Scewon 449-900 South Korea.

10.1021/ma971470p CCC: $15.00
Published on Web 10/30/1998

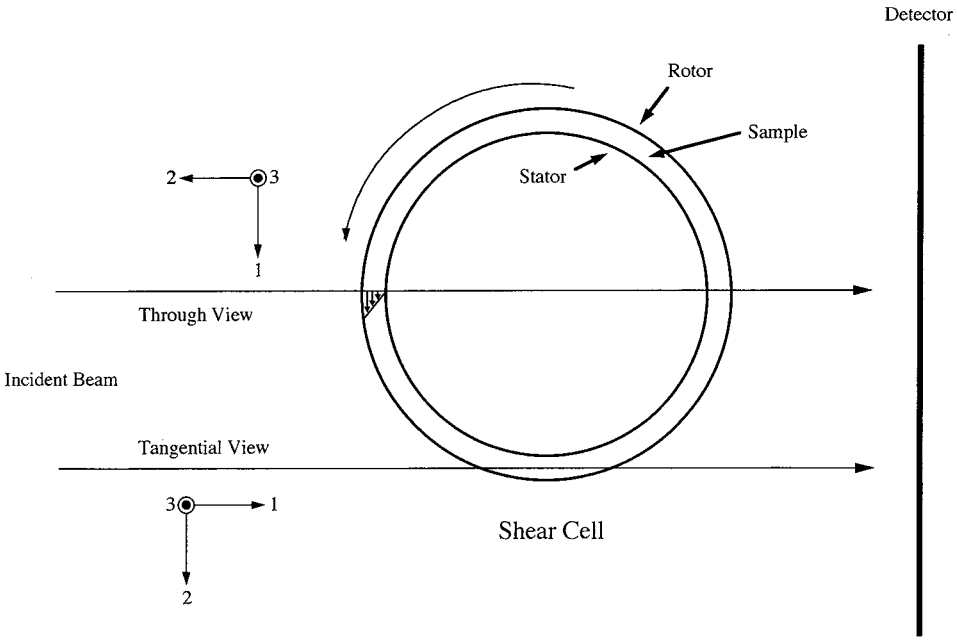

Figure 2. Schematic diagram of the SANS flow cell. The Cartesian coordinate for the shear flow is defined as shown in this figure.

Okamoto et al. reported that polystyrene−poly(ethylene-*alt*-propylene) diblock copolymer exhibits biaxial orientation, i.e., preferentially either "parallel" or "transverse" orientation under particular conditions.[9] Thus, oscillatory shear flow induces preferential lamellar orientation where the orientation direction depends on the experimental conditions.

On the other hand, few studies have been performed under steady shear flow. Balsara et al.[7,8] reported that for PS−PI diblock copolymers in concentrated solutions, steady shear flow makes the lamellar normals reorient from the 1−3 plane to the 2−3 plane. Koppi et al.[20] have reported that "reciprocating steady shear" (with 500% strain amplitude) causes lamellar alignment in the "perpendicular" orientation below T_{ODT} for PEP−PEE diblock copolymers. Moreover, both Balsara et al.[7,8] and Koppi et al.[20] have reported "shear-induced ordering" of lamellae above T_{ODT}.

In this work, we report preliminary results on the study of the influence of steady shear flow on lamellar structures of poly(styrene-d_8-*b*-2-vinylpyridine) diblock copolymer solutions examined by small-angle neutron scattering (SANS) under the flow. Since the rheological behavior of polystyrene and poly(2-vinylpyridine) are quite similar, we may expect different behavior from PS−PI or PEP−PEE.

Experimental Section

Samples. The diblock copolymer samples used here were two symmetric poly(styrene-d_8-*b*-2-vinylpyridine)s, DP19 ($M_w = (2.0 \pm 0.2) \times 10^5$, $M_w/M_n = 1.05$, $\phi_{PS} = 0.52$) and DP20 ($M_w = (3.6 \pm 0.4) \times 10$,[5] $M_w/M_n = 1.08$, $\phi_{PS} = 0.53$), prepared by anionic polymerization and characterized in our laboratory.[21] Here, M_w, M_w/M_n, and ϕ_{PS} denote the weight-average molecular weight,[22] the molecular weight distribution index, and the volume fraction of styrene-d_8, respectively. The solvent used was α-chloronaphthalene (α-CN) from Aldrich,[23] which was used without further purification. α-CN is a common good solvent for both block components.[21,24] The polymer concentrations were 18.1 and 13.5 mass % for DP19 and DP20, respectively.

States of Test Solutions: SANS Measurements without Flow. ODT conditions of symmetric poly(styrene-2-vinylpyridine)s over a wide range of molecular weight in α-CN solutions (at 30 °C) and melts, including DP19 and DP20 solutions, determined by SANS and dynamic rheological measurements (DRM) were already reported.[21] Since the concentrations used in this work were slightly higher than the ODT concentrations at 30 °C (between 17 and 17.5 mass % for DP19 and 10.5−11.5 mass % for DP20), T_{ODT} of the solutions was expected to be higher than 30 °C (estimated to be around 60 °C). To clarify the state of solutions used in this work (ordered or disordered states), we conducted SANS measurements for these solutions with the SANS-U spectrometer at the Neutron Scattering Laboratory of the Institute for Solid State Physics, The University of Tokyo in Tokai, Ibaraki, Japan. The wavelength, λ, was 0.7 nm ($\Delta\lambda/\lambda < 0.15$), the sample to detector distance was 12 m and a 5 mm pinhole was used as the previous work.[21] Measurements were performed every 5 deg from 45 to 70 °C.

SANS Measurements under Steady Shear Flow. SANS measurements under steady shear flow were conducted with the 8 m SANS spectrometer equipped with a two-dimensional position sensitive detector by using a flow cell of the couette type at the Cold Neutron Research Facility of the National Institute of Standards and Technology. The sample−detector distance, the diameter of pinhole, the wavelength, λ, and its distribution, $\Delta\lambda/\lambda$, were 3.6 m, 12 mm, 1.2 nm, and 0.25, respectively, for the DP20 solution, while slightly different conditions, $\lambda = 1.0$ nm and 8 mm pinhole were used for the DP19 solution. Scattering data were obtained as a function of the magnitude of the scattering vector, q, defined by $q = 4\pi \sin(\theta/2)/\lambda$, where θ is scattering angle. Details of the flow cell were described in a previous paper.[25] It should be noted that the collimation condition for SANS under the flow was not as good as that of SANS-U, but it does not seriously affect the results reported in this work.

The measurement was started from the lowest measuring temperature (25 °C) and successively increased to the highest ones (DP19, 65 °C, DP20, 55 °C). Before moving to the higher measuring temperature, the cell temperature was held at 70 °C (see below) for 5 min to erase the previous shear history, and then gradually cooled to the next measuring temperature by turning off the heater for the DP20 solution. This procedure was not done for the DP19 solution since there was no detectable shear effect for this sample, as shown later. Flow was applied when the measuring temperature was reached (Generally, it took about 5 min for the last 1 °C change). The shear rate was increased stepwise from the lowest shear rate

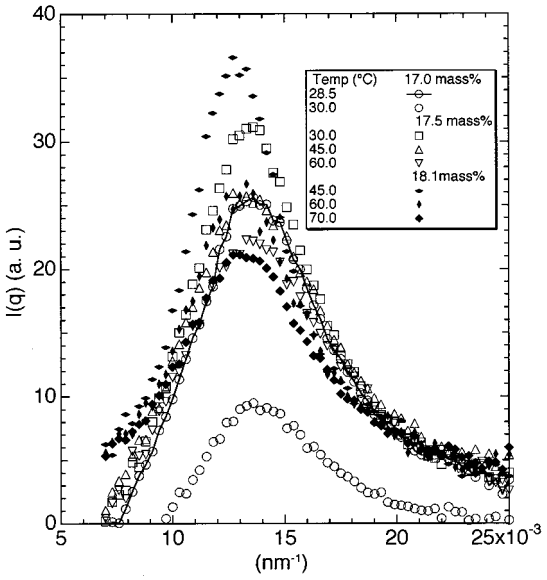

Figure 3. Plots of $I(q)$ vs q for DP19 solutions. Concentrations and temperatures are denoted in the figure. Filled symbols denote the data in this work, while open symbols are data obtained in the previous work.[21]

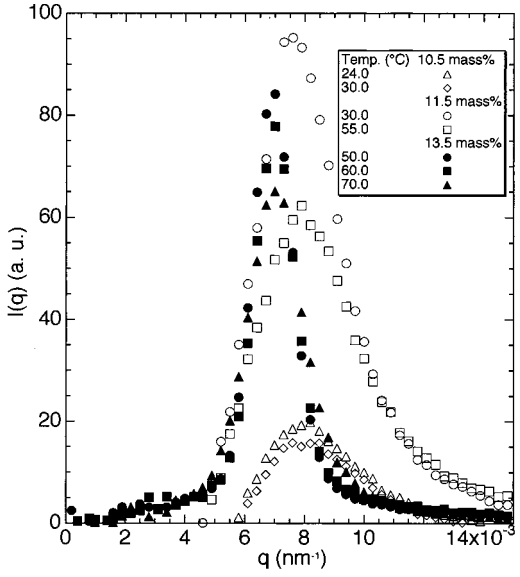

Figure 4. Plots of $I(q)$ vs q for DP20 solutions. Concentrations and temperatures are denoted in the figure. Filled symbols denote the data in this work, while open symbols are data obtained in the previous work.[21]

to the highest shear rate. The measurements were started about 5 min after the flow was started.

SANS measurements were taken in two different directions called the "through view" and the "tangential view", as shown in Figure 2. The neutron beam is parallel to the shear gradient, i.e., the 2-direction, in the through view, while it is parallel to the flow direction, i.e., the 1-direction, in the tangential view. The beam position was confirmed by taking neutron beam photography. For the through view, we neglected the curvature of the cell and the difference in scattering positions caused by the fact that the incident beam passes through the sample cell twice, because the sample−detector distance is much longer than the couette diameter. Since the scattering volume and the thickness of the cell were unknown and the scattering from the cell itself was quite large in the tangential view, the tangential view data are used for qualitative discussion only.

The scattering intensities in the through view were converted to absolute intensities using a silica gel standard. The incoherent scattering of the solvent, poly(2-vinylpyridine) and the empty cell were subtracted from the scattering intensity by considering their volume fraction in the solution. The contribution of the incoherent scattering of the polystyrene-d_8 was neglected. For the following discussion we define the azimuthal angle, ϕ, on the contour maps as the counterclockwise rotation angle from $\phi = 0°$ at the 1-direction in the through view and at the 2-direction in the tangential view (see Figures 5 and 8). It should be noted that all the contour maps of scattering intensity shown in this paper are uncorrected "raw" data.

Results

State of Test Solutions. For the DP19 solution, an isotropic scattering pattern was observed on the two-dimensional detector at all the temperatures examined so that the data were corrected for background and incoherent scattering of the solvent and the circularly averaged intensity $I(q)$ was obtained as in previous work.[21] For the DP20 solution, on the other hand, a weak anisotropy of the scattered intensity, due to the alignment of the structure induced when the sample solution was put into the quartz cell, was observed on the two-dimensional detector up to 65 °C through the measurement. However, the anisotropy disappeared soon after the temperature was elevated to 70 °C. After

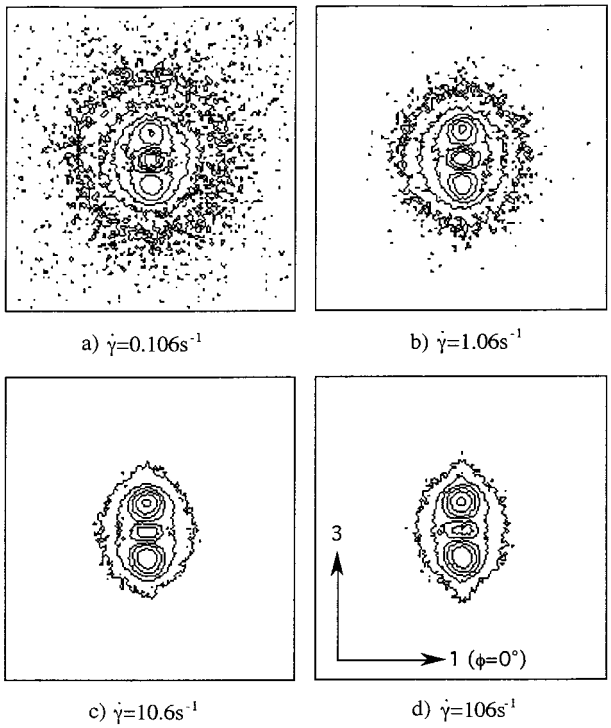

Figure 5. Contour maps of SANS in the through view at 35 °C at various shear rates. The contour lines are drawn with the same intervals of intensity in all the maps, so that the intensities can be qualitatively compared with each other.

the measurement at 70 °C, we again measured at 65 °C and confirmed that the circularly averaged intensities $I(q)$ with and without anisotropy at 65 °C do not differ so much, so that we also use $I(q)$ for all the data of DP20, neglecting the anisotropy.

Figures 3 and 4 shows examples of plots of $I(q)$ vs q for DP19 and DP20 solutions, respectively. Filled symbols denote the data in this work, while open symbols denote the data in previous work[21] (though not all of them were reported previously). In Figure 3, it is clear that all the data for the 17.5 mass % solution and 17.0 mass % solution at 28.5 °C are similar, though the

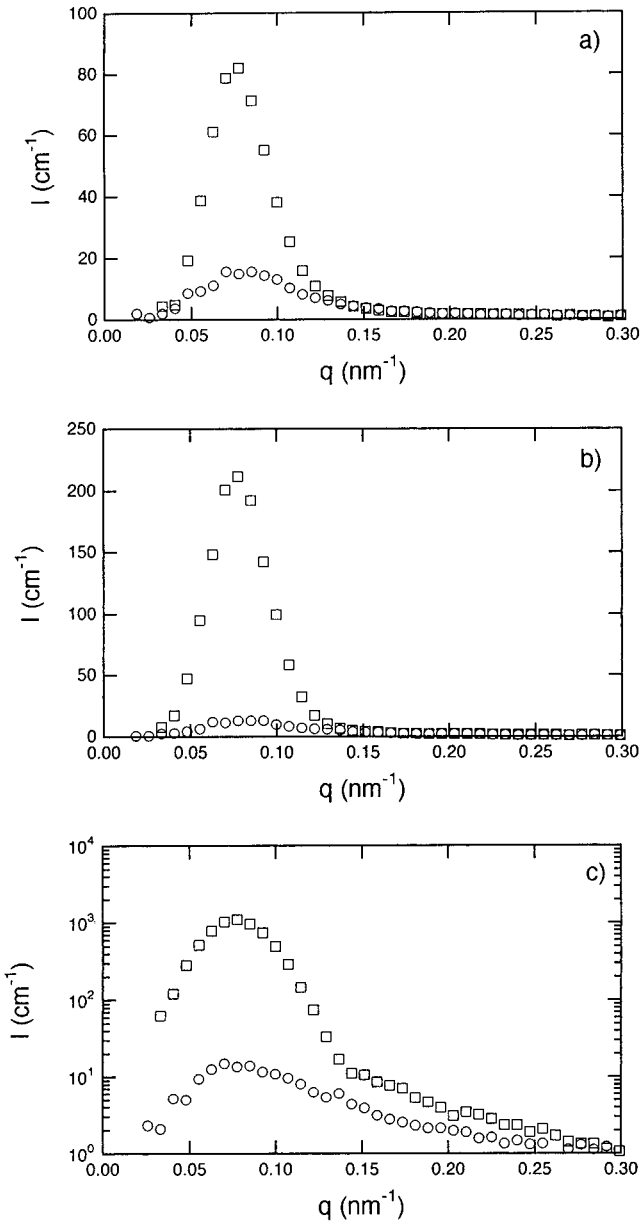

Figure 6. Sector-averaged intensity profiles at $\phi = 0$ and 180° (circles) and $\phi = 90$ and 270° (squares) (sector ±10°) in the through view at 35 °C at various shear rates: (a) $\dot{\gamma} = 0.106$, (b) 1.06, and (c) 10.6 s^{-1}. Relative standard uncertainties are at most 7% around the peak position ($q = 7.8 \times 10^{-2}$ nm^{-1}).

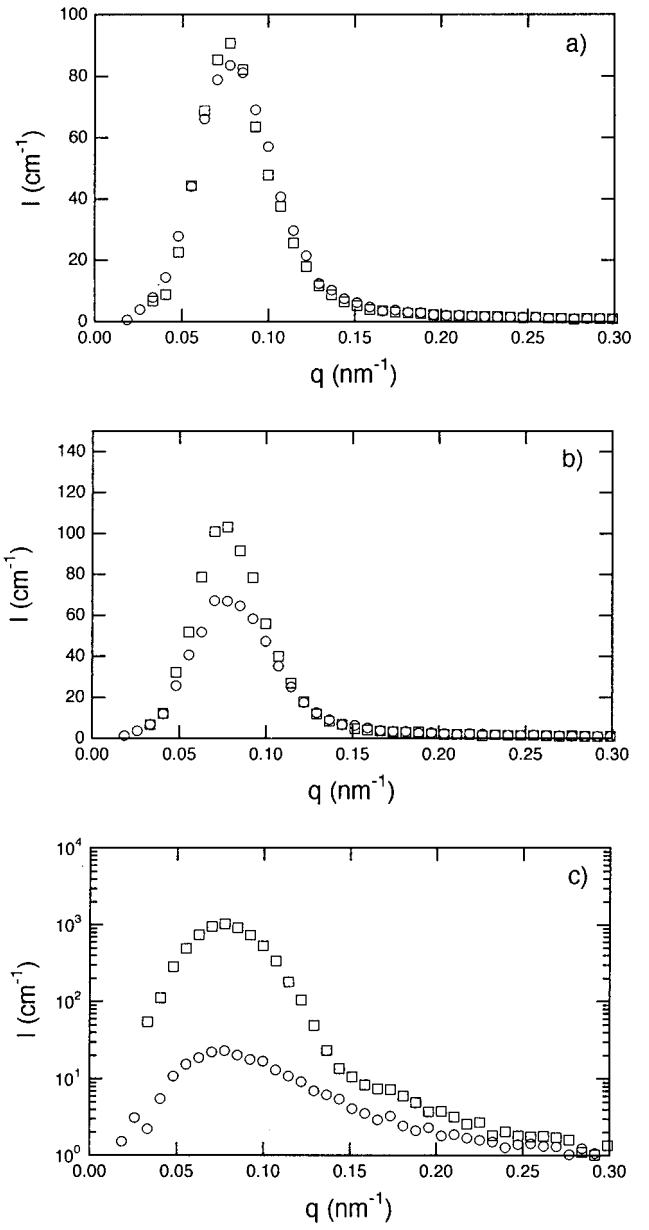

Figure 7. Sector-averaged intensity profiles at $\phi = 0$ and 180° (circles) and $\phi = 90$ and 270° (squares) (sector ±10°) in the through view at 45 °C at various shear rates: (a) $\dot{\gamma} = 1.08$, (b) 10.8, and (c) 108 s^{-1}. Relative standard uncertainties are at most 7% around the peak position ($q = 7.8 \times 10^{-2}$ nm^{-1}).

peak position and peak height change with a change of concentration and temperature. When the temperature was raised from 28.5 to 30.0 °C for the 17.0 mass % solution, $I(q)$ data drastically changed (circles with and without line). Since the DRM data also changed from the behavior of ordered state to that of disordered state at almost the same condition, we determined the ODT condition as 17.0−17.5 mass % for DP19 at 30 °C. Comparing the $I(q)$ data for the 18.1 mass % solution with other data, it is clear that all are similar to those in the ordered state, though the peak position and peak height gradually change with a change of concentration and temperature.

In Figure 4, the data for the 11.5 mass % solution gradually changed with the change of temperature but did not show the change corresponding to ODT observed in Figure 3. However, with a small change of concentration to 10.5 mass %, the $I(q)$ data drastically changed as in Figure 3. Together with the change in DRM data, the ODT concentration for DP20 was determined as 10.5−11.5 mass % at 30 °C. It is also clear that $I(q)$ data for the 13.5 mass % solution show the scattering of the ordered state up to 70 °C, as the 11.5 mass % solution. Thus, without further analysis, we conclude that T_{ODT} of DP19 and DP20 solutions tested in this work are higher than 70 °C and we can safely assume that our results discussed below are in the ordered state.

SANS Results under Flow. Figure 5 shows examples of contour maps of the two-dimensional detector in the through view in SANS measurements under shear flow at 35 °C. On these contour maps, the anisotropy in the Bragg diffraction peaks becomes stronger as $\dot{\gamma}$ increases. Figures 6 and 7 show examples of sector-averaged (sector = ±10°) intensity profiles in the through view along the 1-direction ($\phi = 0$ and 180°) and the 3-direction ($\phi = 90$ and 270°) at various $\dot{\gamma}$ values

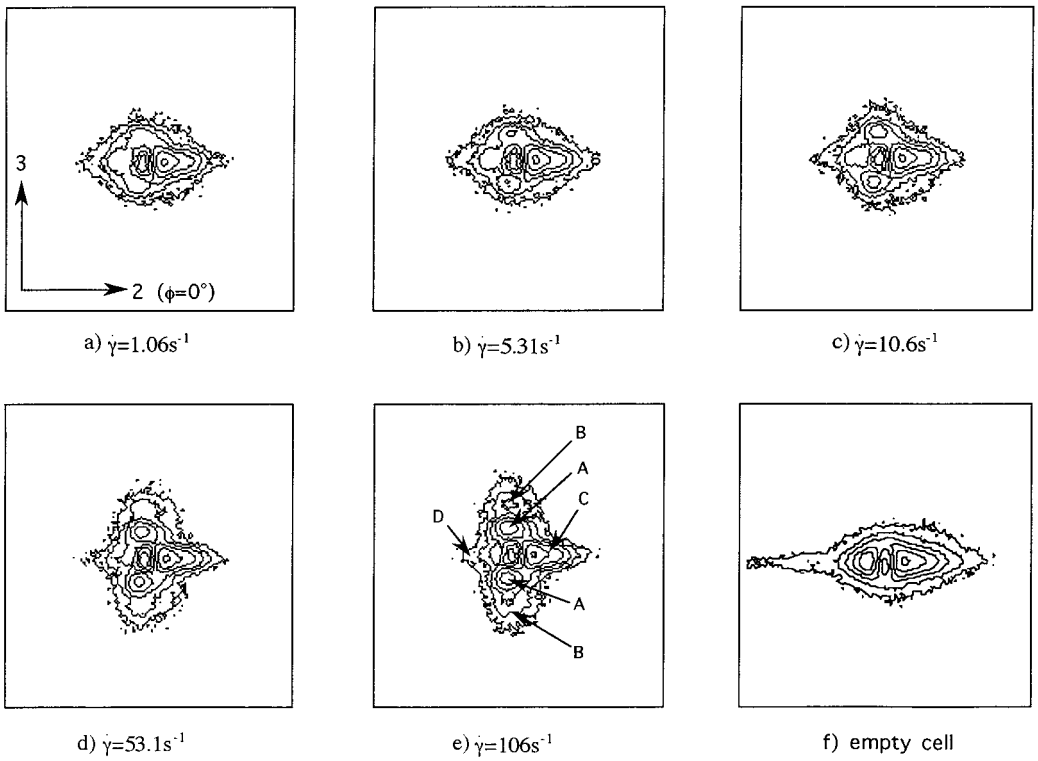

Figure 8. Contour maps of SANS in the tangential view at 35 °C at various shear rates. (f) shows empty cell scattering. The contour lines are drawn with the same intervals of intensity in all the maps.

at 35 and 45 °C, respectively. In these figures, we can see a single peak in each intensity profile around $q = 7.8 \times 10^{-2}$ nm^{-1}, which corresponds to the lamellar domain spacing. Hereafter, we refer to the peak intensities of sector-averaged plots at $\phi = 0$ and 180° and $\phi = 90$ and 270° in the through view as $I_{max,h}$ and $I_{max,v}$ which indicate the "transverse" and "perpendicular" orientations, respectively. At 35 °C, there is a significant difference between $I_{max,h}$ and $I_{max,v}$ at low shear rates (Figure 6a). This difference increases with increasing $\dot{\gamma}$ as shown in Figure 6b,c. At 45 °C, there is almost no difference between $I_{max,h}$ and $I_{max,v}$ at low shear rates (Figure 7a), but with increasing $\dot{\gamma}$ (Figures 7b and c), $I_{max,v}$ increases, while $I_{max,h}$ decreases simultaneously. A shoulder appears around $q = 2(7.8 \times 10^{-2})$ nm^{-1} in the intensity profiles of $I_{max,v}$ at very high shear rates at both temperatures (Figures 6c and 7c), indicating strong "perpendicular" orientation.

Figure 8 shows examples of contour maps in the tangential view at 35 °C. We find a pair of spots in the 3-direction ($\phi = 90$ and 270°) at 7.8×10^{-2} nm^{-1}, as indicated by A in Figure 8e, which become stronger as $\dot{\gamma}$ increases. Moreover, the second peaks indicated by B are more clearly observed in the tangential view than in the through view, indicating also the strong "perpendicular" orientation. A very strong scattering at $\phi = 0°$ indicated by C, is primarily due to the cell itself. The peak at $\phi = 180°$, indicated by D also contains scattering from the cell, but the intensity decreases with increasing $\dot{\gamma}$, indicating that this peak includes the diffraction from lamellae with normals that are oriented along the direction parallel to the 2-direction. In other words, the "parallel" orientation decreases with increasing $\dot{\gamma}$.

Figure 9 shows plots of $I_{max,h}$ and $I_{max,v}$ against $\dot{\gamma}$ at 25, 35, 45, and 55 °C. The difference between $I_{max,h}$ and $I_{max,v}$ increases with increasing $\dot{\gamma}$ at all temperatures,

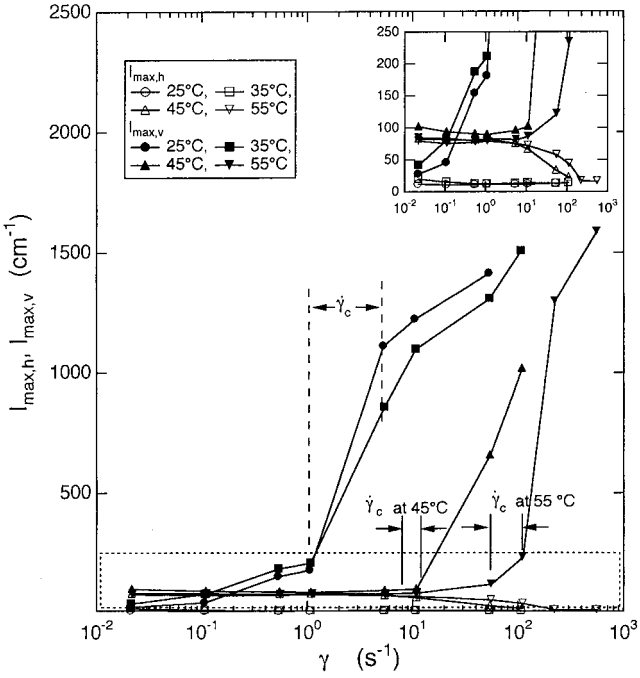

Figure 9. Shear rate dependencies of $I_{max,h}$ and $I_{max,v}$. The area surrounded by a broken line is expanded in the inset figure. $\dot{\gamma}_c$ is the characteristic shear rate (see text.). Relative standard uncertainties are at most 7% for all the data.

but their shear rate dependencies are quite different between the data at 25 and 35 °C and at 45 and 55 °C. At 25 and 35 °C, the $I_{max,h}$ and $I_{max,v}$ values are slightly but significantly different even at low shear rates (cf. Figure 6a), and both are smaller than the data at 45 and 55 °C at the low shear rates. The $I_{max,v}$ curves at 25 and 35 °C increase steeply at $\dot{\gamma} = 1-5$ s^{-1}, while the

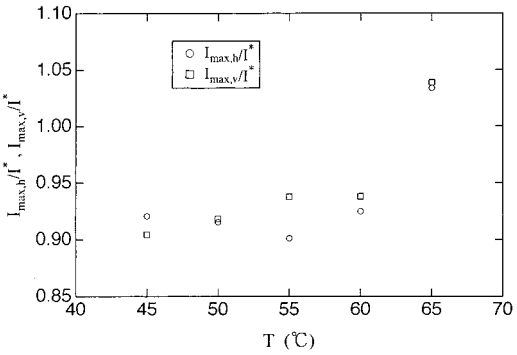

Figure 10. Plots of $I_{max,h}$/I* and $I_{max,v}$/I* vs T for DP19 solutions at $\dot{\gamma} = 1000\ s^{-1}$.

$I_{max,h}$ values are almost unchanged. At 45 and 55 °C, on the other hand, the $I_{max,h}$ and $I_{max,v}$ values are almost equal at low shear rates, and the former increases but the latter decreases simultaneously around $\dot{\gamma} = 10\ s^{-1}$.

In contrast to these observations for DP20 solution, no apparent effects of flow were observed for the DP19 solution. Figure 10 shows plots of $I_{max,h}/I^*$ and $I_{max,v}/I^*$ against T at the highest shear rate ($\dot{\gamma} = 1000\ s^{-1}$) tested for DP19, where I^* denotes the circularly averaged peak intensity without flow obtained in the shear cell. The data are scattered around unity, but there ranges are practically the same as those of corresponding data without shear (±10%). The peak position was also not changed by the flow.

Discussion

The above results reveal that the steady shear flow does not induce a morphological transition, in contrast to a previous work,[15] but instead influences the lamellar orientation for DP20 in α-CN. On the other hand, no shear effect was observed for DP19 solution. Therefore, hereafter, we mainly discuss the data of DP20. Roughly speaking, with increasing $\dot{\gamma}$, the lamellae assuming "perpendicular" orientation increase, while those assuming the other orientations decrease. The results also indicate that the lamellar domain spacing is almost unchanged during the orientation process.

From the results for DP20 solution, we construct a temperature−shear rate diagram for the scattering patterns in the through view, as shown in Figure 11. We can define three regimes according to the observed scattering patterns. Regime I is the isotropic ring regime, in which an isotropic circular peak was observed in the through view. Regime II is the anisotropic peak regime, in which the scattering intensity at $q = 7.8 \times 10^{-2}$ nm^{-1} shows anisotropy but the second peaks (shoulders) are not observed yet in the through view. Regime III is the anisotropic peak regime, in which the scattering anisotropy is very strong and the second peaks are observed in the through view. The characteristic shear rate $\dot{\gamma}_c$, which divides the diagram into regime I and III or regime II and III, is shown in Figure 11. At low shear rates ($\dot{\gamma} = 10^{-2}$ - 1 s^{-1}), moreover, we observe a characteristic temperature, T_c, which is nearly constant between 37.5 and 40 °C, dividing the diagram into regimes I and II. Above T_c, $\dot{\gamma}_c$ increases with increasing temperature and it divides the diagram into regimes I and III. Below T_c, $\dot{\gamma}_c$ exists between 1 and 5 s^{-1} and it divides the diagram into regimes II and III.

For $T < T_c$, the $I_{max,h}$ values are fairly suppressed over all the $\dot{\gamma}$ regions, as shown in Figure 9. This result implies that the number of lamellae with normals

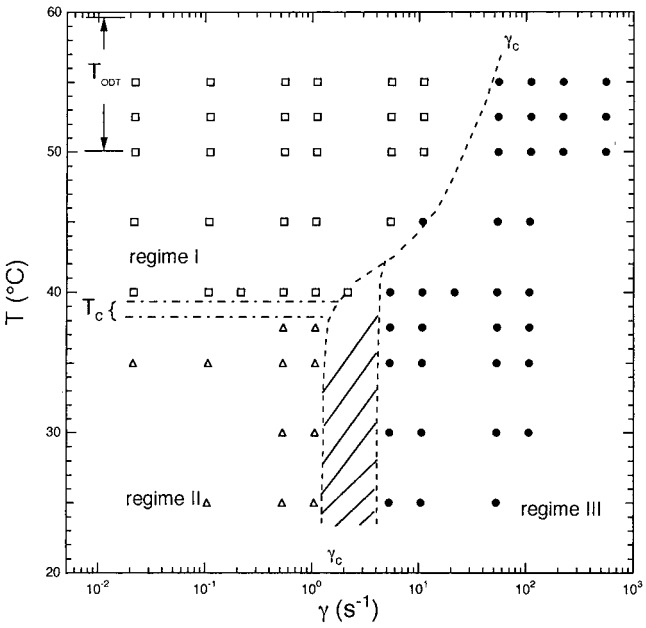

Figure 11. Temperature−shear rate diagram for lamellar orientation and ordering obtained in the through view. The dashed curve and the shaded area represent $\dot{\gamma}_c$.

oriented along the direction parallel to the 1-direction (the "transverse" orientation) is reduced. The increase in $I_{max,v}$ at $\dot{\gamma} < \dot{\gamma}_c$ implies that the number of lamellae with normals oriented along the direction parallel to the 3-direction (the "perpendicular" orientation) increases with increasing $\dot{\gamma}$. As shown in the inserted figure, the $I_{max,v}$ values at 25 and 35 °C ($< T_c$) are lower than the isotropic intensity at 45 and 55 °C ($> T_c$) at low shear rates ($\dot{\gamma} \leq 10^{-1}\ s^{-1}$). This implies the existence of certain amounts of lamellae with normals parallel to the 2-direction. Balsara et al.[7] reported that the steady shear reorients the lamellar normals from the 1−3 plane to the 2−3 plane below T_{ODT}. We also think this is the case at $\dot{\gamma} < \dot{\gamma}_c$. Moreover, they reported that steady shear is not sufficient to orient the lamellae of the SI block copolymer solution.[7] However, we found that the $I_{max,v}$ values steeply increase at $\dot{\gamma}_c$, whereas the $I_{max,h}$ values are unchanged. This implies that the lamellae are oriented from the coexisting state where the lamellar normals lie in the 2−3 plane to the "perpendicular" direction. The appearance of a second peak at $q = 2(7.8 \times 10^{-2})$ nm^{-1} (Figures 5, 6, and 8) also implies the predominant orientation of the lamellae in the "perpendicular" orientation. This change at $\dot{\gamma}_c$ is also evidence that the lamellae with normals that lie in the 2−3 plane (except for the "perpendicular" orientation) exist at $\dot{\gamma} < \dot{\gamma}_c$.

Under oscillatory shear flow, Koppi et al.[3] reported that the "parallel" orientation was achieved over a wide range of frequency. They suggested that the "parallel" orientation is produced for PEP−PEE diblock copolymer in bulk at low frequencies by the motion of defects to relax the stress focused on the grains oriented fully or partly along the "transverse" directions. This is essentially the same idea as the "rocking" mechanism suggested by Kannan and Kornfield.[4] However, for the present sample under steady shear flow, the "parallel" orientation decreases with increasing $\dot{\gamma}$ even in regime II. To understand this result, it should be noted that the rotational flow component in the steady shear flow is one of the most important factors for determining the lamellar orientation. Even if all the lamellae were to

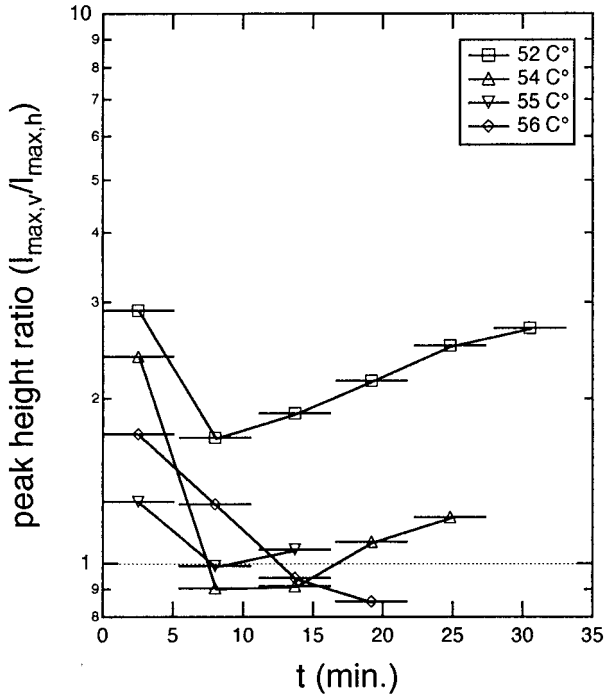

Figure 12. Relaxation of anisotropy of intensity in the through view after the cessation of shear rate (at $t = 0$) of ca. 100 s^{-1}. Relative standard uncertainties are at most 7% for both $I_{max,h}$ and $I_{max,v}$.

be in the "parallel" orientation, they would continue to rotate under steady shear flow, so that the "parallel" orientation would not have any advantage over the "transverse" orientation, in contrast to oscillatory shear flow. The idea that the continuous rotational component strongly affects the orientation is consistent with the fact that the strain amplitude is one of the most important factors for lamellar orientation under oscillatory shear flow.[3]

In regime I ($T > T_c$), isotropic scattering was observed in the through view as shown in Figure 8. This result is similar to that of the DP19 solution, but the temperature and shear rate range are limited. It is difficult to identify whether this region is an ordered or disordered state by this flow SANS experiment. There is a possibility that there exists a small anisotropy in regime I and DP19 solutions. More precise measurements are needed to obtain a definite conclusion about these problems.

Above $\dot{\gamma}_c$, the $I_{max,h}$ values decrease, but the $I_{max,v}$ values increase to almost the same magnitudes as at 25 and 35 °C ($< T_c$). Thus, it is concluded that the "perpendicular" orientation is attained for $\dot{\gamma} \geq \dot{\gamma}_c$ even when $T > T_c$.

Finally, we mention the behavior after cessation of flow. Figure 12 shows the relaxation behavior of the anisotropy of scattering ($I_{max,v}/I_{max,h}$) after cessation of shear flow of ca. 100 s^{-1} at several temperatures. As shown in Figure 12, the $I_{max,v}/I_{max,h}$ values decrease to unity (isotropic scattering) within 15 min at 54, 55, and 56 °C, while they did not decrease to unity over the duration of the experiment (anisotropic scattering) at 52 °C. The difference in the observations by SANS-U and 8 m SANS may be due to the difference in collimation conditions. There may exist a small anisotropy at higher temperatures. Even so, these facts may imply that the stability of an aligned structure has a strong temperature dependence.

Summary

In this work, we studied the effects of steady shear flow on the microdomain structures of two ordered symmetric diblock copolymer solutions in a common good solvent. There was almost no effect of flow for a lower molecular weight sample solution, DP19/α-CN solution, which we cannot explain at this stage. On the other hand, we observed lamellae orientation by steady shear flow and presented the temperature-shear rate diagram for a DP20/α-CN solution. The results are summarized as follows.

1. $T < T_c$: At $\dot{\gamma} < \dot{\gamma}_c$, the lamellae with normals lying in the 2−3 plane exist (regime II; coexistent state of Balsara et al.[7]). With increasing $\dot{\gamma}$, the "perpendicular" orientation increases and eventually it becomes dominant at $\dot{\gamma} \geq \dot{\gamma}_c$ (regime III).

2. $T > T_c$: At $\dot{\gamma} < \dot{\gamma}_c$, the isotropic scattering is observed (regime I), while the "perpendicular" orientation becomes dominant at $\dot{\gamma} \geq \dot{\gamma}_c$ (regime III).

A region where the "parallel" orientation is dominant was not observed, in contrast with oscillatory shear flow. Above $\dot{\gamma}_c$, the lamellae orient from the coexistent state to the "perpendicular" orientation at $T < T_c$. This phenomena has not been reported previously. More systematic studies combined with rheological measurements are under progress, and the results will be reported in near future.

References and Notes

(1) Bates, F. S.; Rosedale, J. H.; Fredrickson, G. H. *J. Chem. Phys.* **1990**, *92*, 6225.
(2) Riise, B. L.; Fredrickson, G. H.; Larson, R. G.; Pearson, D. S. *Macromolecules* **1995**, *28*, 7653.
(3) Koppi, K. A.; Tirrell, M.; Bates, F. S.; Almdal, K.; Colby, R. H. *J. Phys. II Fr.* **1992**, *2*, 1941.
(4) Kannan, R. M.; Kornfield, J. A. *Macromolecules* **1994**, *27*, 1177.
(5) Winey, K. I.; Patel, S. S.; Larson, R. G.; Watanabe, H. *Macromolecules* **1993**, *26*, 2542.
(6) Winey, K. I.; Patel, S. S.; Larson, R. G.; Watanabe, H. *Macromolecules* **1993**, *26*, 4373.
(7) Balsara, N. P.; Hammouda, B.; Kesani, P. K.; Jonnalagadda, S. V.; Straty, G. C. *Macromolecules* **1994**, *27*, 2566.
(8) Balsara, N. P.; Dai, H. J.; Kesani, P. K.; Garetz, B. A.; Hammouda, B. *Macromolecules* **1994**, *27*, 7406.
(9) Okamoto, S.; Saijo, K.; Hashimoto, T. *Macromolecules* **1994**, *27*, 5547.
(10) Zhang, Y.; Wiesner, U.; Spiess, H. W. *Macromolecules* **1995**, *28*, 778.
(11) Zhang, Y.; Wiesner, U.; Yang, Y.; Pakula, T.; Spiess, H. W. *Macromolecules* **1996**, *29*, 5427.
(12) Hadziioannou, G.; Mathis, A.; Scoulios, A. *Colloid Polym. Sci.* **1979**, *257*, 136.
(13) Morrison, F. A.; Mays, J. W.; Muthukumar, M.; Nakatani, A. I.; Han, C. C. *Macromolecules* **1993**, *26*, 5271.
(14) Jackson, C. L.; Barnes, K. A.; Morrison, F. A.; Mays, J. W.; Nakatani, A. I.; Han, C. C. *Macromolecules* **1995**, *28*, 713.
(15) Nakatani, A. I.; Morrison, F. A.; Douglas, J. F.; Mays, J. W.; Jackson, C. L.; Muthukumar, M.; Han, C. C. *J. Chem. Phys.* **1996**, *104*, 1589.
(16) Morrison, F. A.; LeBourvellec, G.; Winter, H. H. *J. Appl. Polym. Sci.* **1987**, *33*, 1585.
(17) Morrison, F. A.; Winter, H. H. *Macromolecules* **1989**, *22*, 3533.
(18) Morrison, F. A.; Winter, H. H.; Gronski, W.; Barnes, J. D. *Macromolecules* **1990**, *23*, 4200.
(19) Scott, D. B.; Waddon, A. J.; Lin, Ye-Gang; Karasz, F. E.; Winter, H. H. *Macromolecules* **1992**, *25*, 4175.
(20) Koppi, K. A.; Tirrell, M.; Bates, F. S. *Phys. Rev. Lett.* **1993**, *70*, 1449.
(21) Takahashi, Y.; Kitade, S.; Noda, M.; Ochiai, N.; Noda, I.; Imai, M.; Matsushita. Y. *Polym. J.* **1998,** 30, 388.
(22) According to ISO 31-8, the term "Molecular Weight" has been replaced by "Relative Molecular Mass", symbol M_r. Thus, if this nomenclature and notation were to be followed in this

publication, one would write $M_{r,n}$ instead of the historically conventional M_n for the number average molecular weight, with similar changes for M_w, and it would be called the "Number Average Relative Molecular Mass." The conventional notation, rather than the ISO notation, has been employed for this publication.

(23) Certain equipment, instruments or materials are identified in this paper in order to adequately specify the experimental details. Such identification does not imply recommendation by the National Institute of Standards and Technology nor does it imply the materials are necessarily the best available for the purpose.

(24) Takahashi, Y.; Ochiai, N.; Matsushita. Y.; Noda, I. *Polym. J.* **1996**, *28*, 1065.

(25) Nakatani, A. I.; Kim, H.; Han, C. C. *J. Res. Natl. Inst. Stand. Technol.* **1990**, *95*, 7.

MA971470P